Electronic Supplementary Information

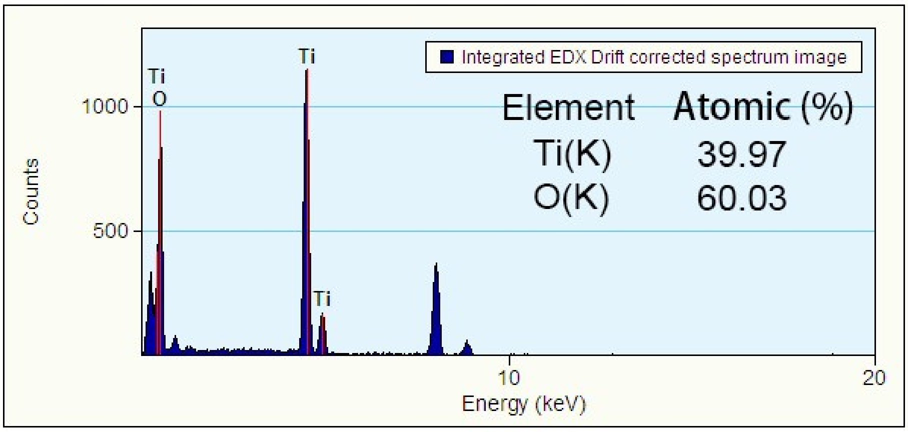

Fig. S1. Integrated EDX drift corrected spectrum of d-TiO_2.

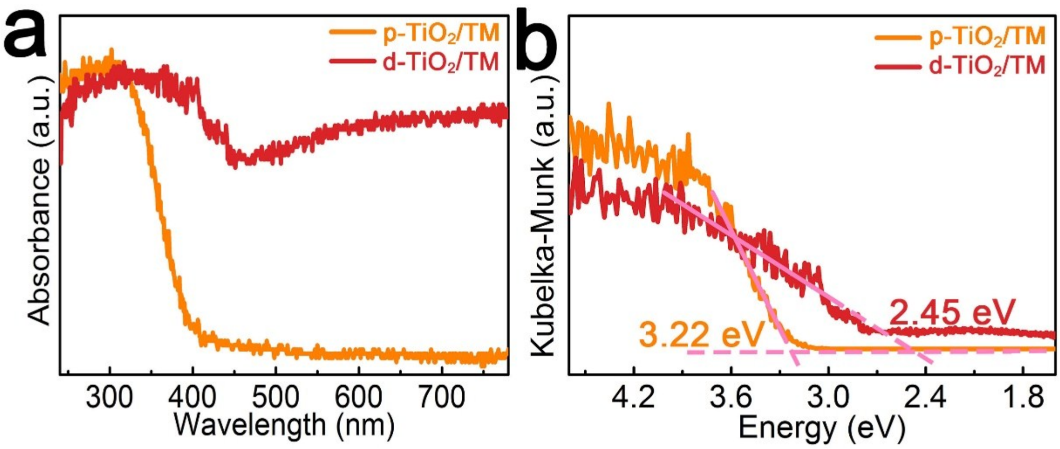

Fig. S2. (a) UV-vis absorption spectra of p-TiO_2 and d-TiO_2.(b) Corresponding plots of the transformed Kubelka-Munk function against light energy for p-TiO_2 and d-TiO_2.

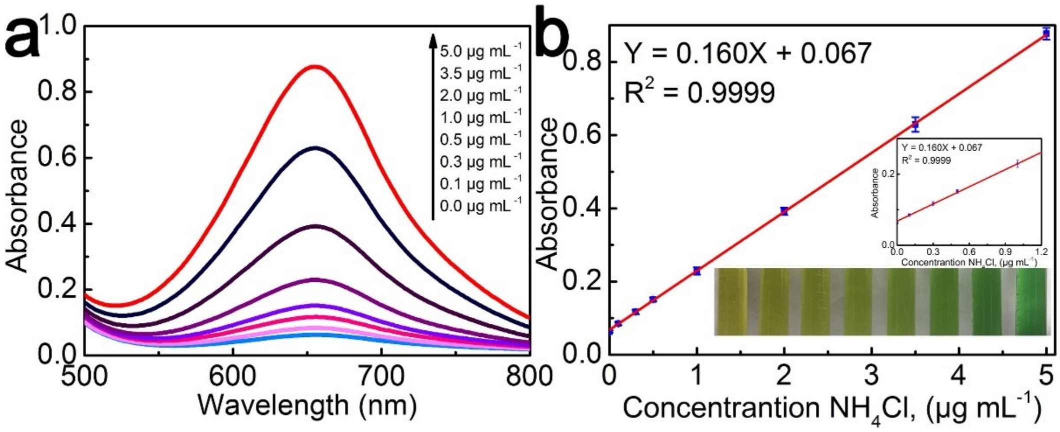

Fig. S3. (a) UV-Vis absorption spectra of indophenol assays with NH_4Cl after incubated for 2 h at room temperature. (b) Calibration curve used for estimation of NH_4Cl (inset: amplification of the concentration ranges from 0.0 to 1.0 μg).

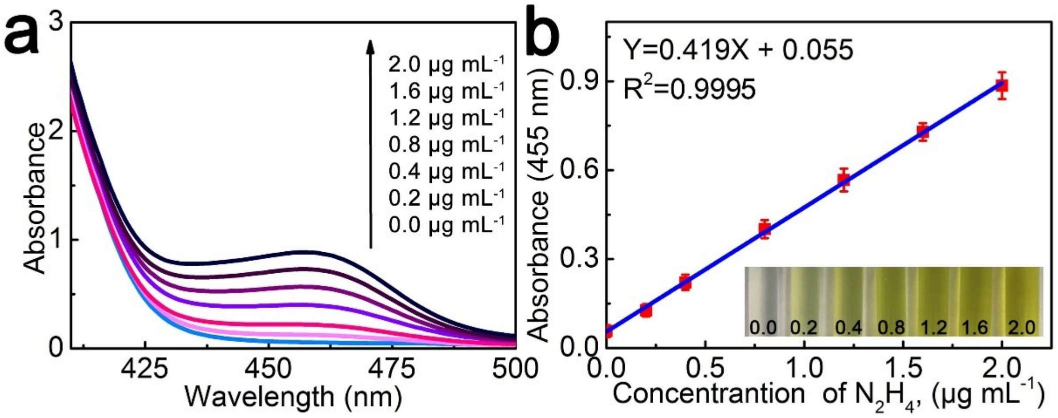

Fig. S4. (a) UV-Vis absorption spectra of various N_2H_4 concentrations after incubated for 15 min at room temperature. (b) Calibration curve used for calculation of N_2H_4 concentrations. Error bar associated with each value is also provided.

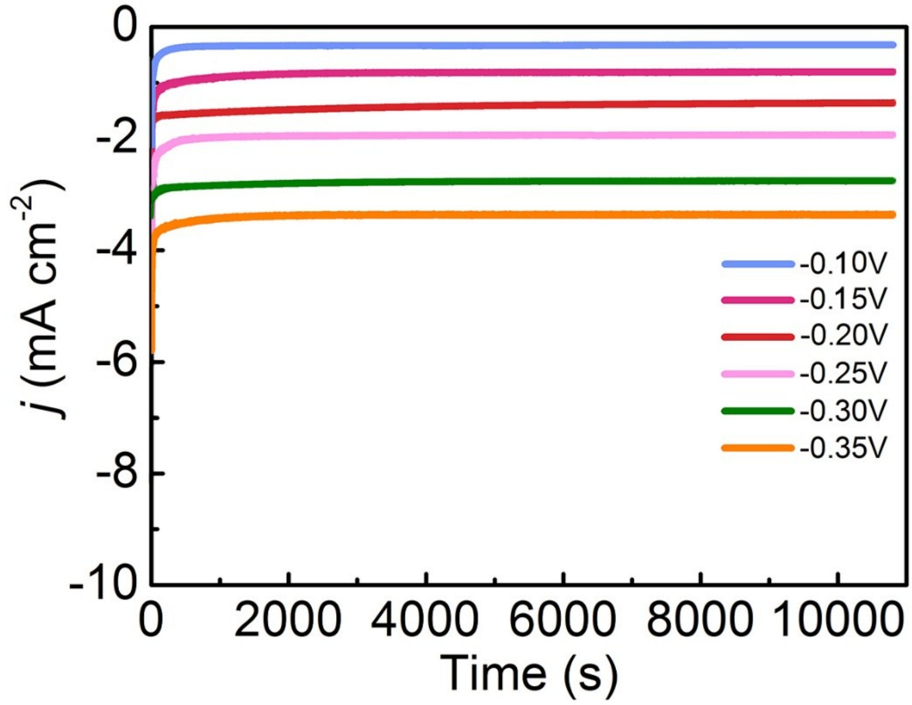

Fig. S5. Chronoamperometric data of d-TiO_2/TM for NRR at each given potential. All experiments were carried out in 0.1 M HCl at room temperature and ambient pressure.

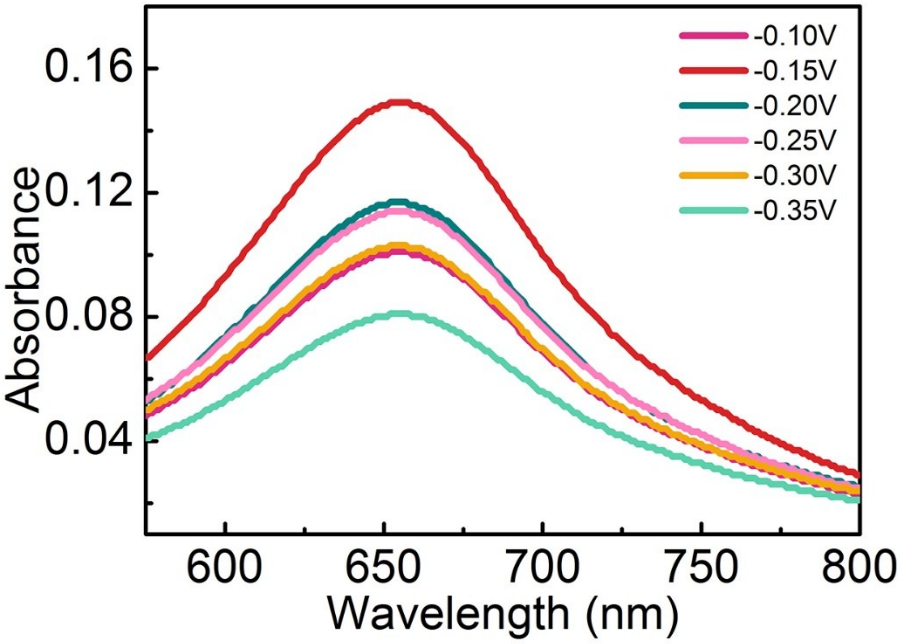

Fig. S6. UV-Vis absorption spectra of the electrolytes stained with indophenol indicator after NRR electrolysis at each given potential. All experiments were carried out in 0.1 M HCl at room temperature and ambient pressure.

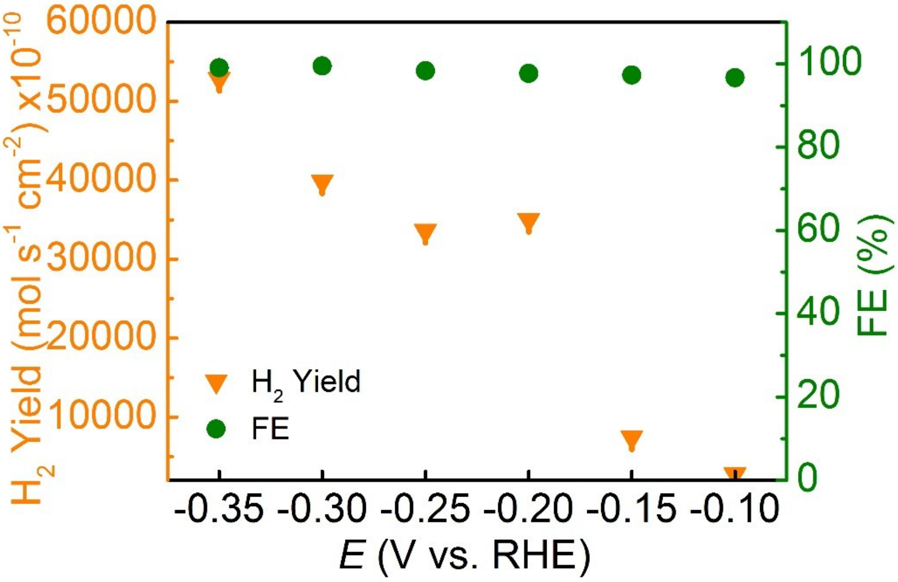

Fig. S7. H_2 yields and FEs at each given potential in Ar-saturated electrolytes using d-TiO_2/TM as electrode.

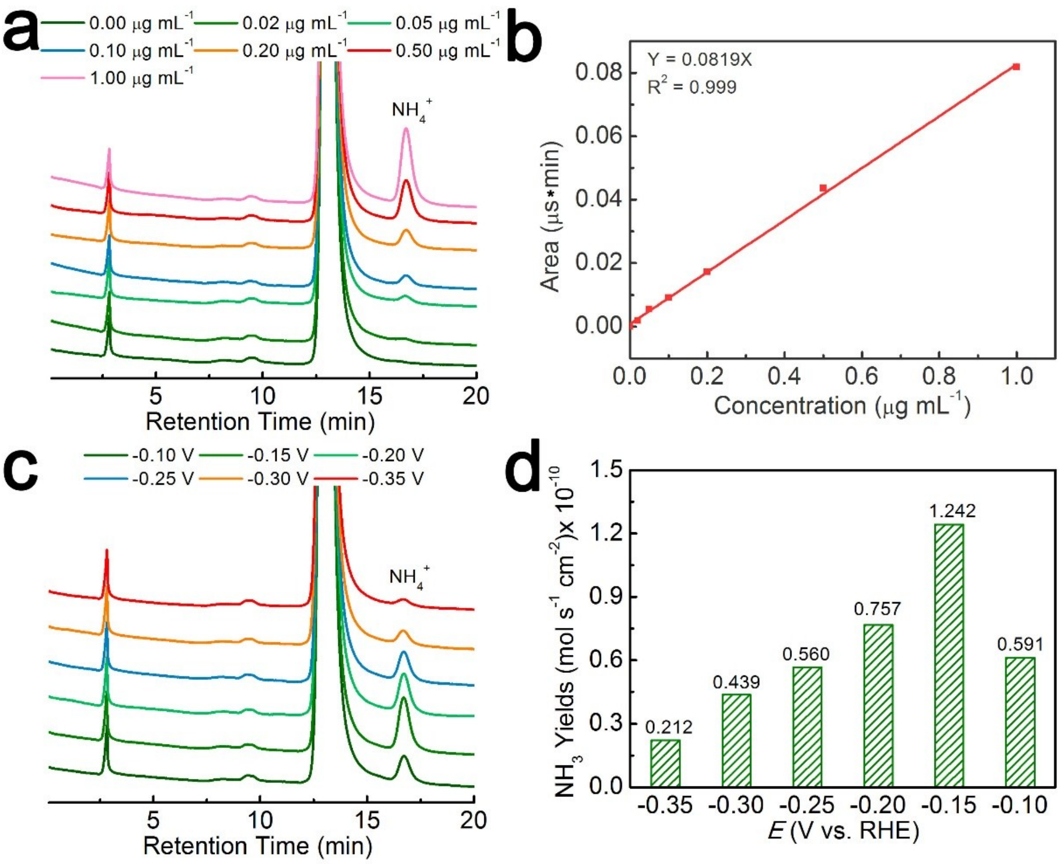

Fig. S8. (a) Ion chromatograms of NH_4Cl with different concentrations in 0.1 M HCl and (b) corresponding standard curve for NH_4Cl contents. (c) Ion chromatograms for the electrolyte after the electrolysis at different potentials. (d) NH_3 yields calculated via the standard curve in (b).

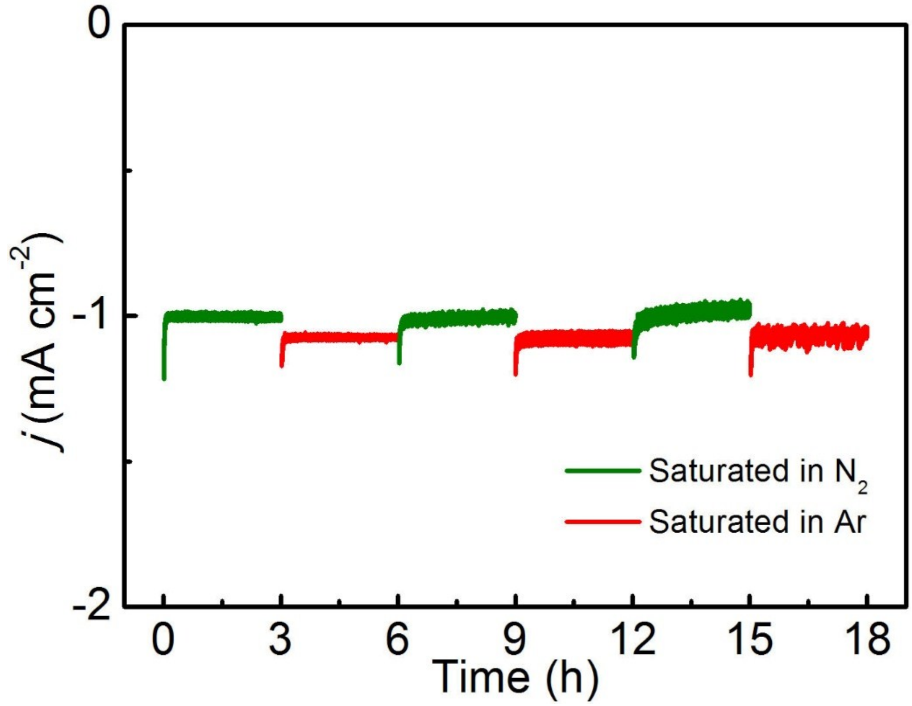

Fig. S9. Chronoamperometric data for d-TiO_2/TM with alternating 3-h cycles between N_2-saturated and Ar-saturated electrolytes for a total of 18h at –0.15 V.

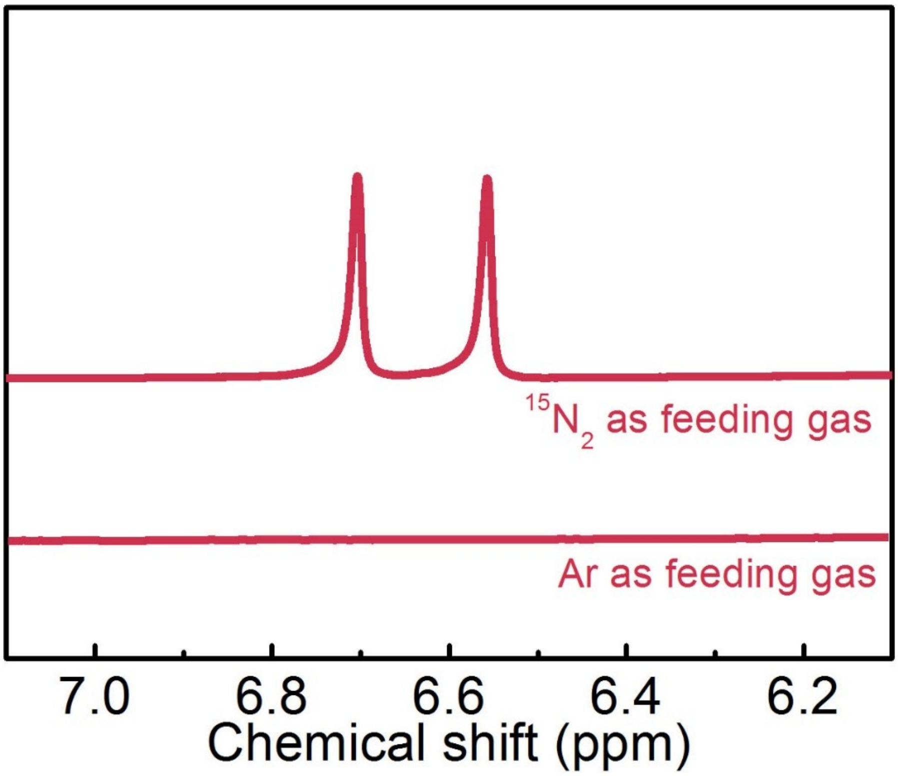

Fig. S10. 1H NMR spectra of $^{15}NH_4^+$ produced from the NRR reaction with Ar and $^{15}N_2$ as feeding gass.

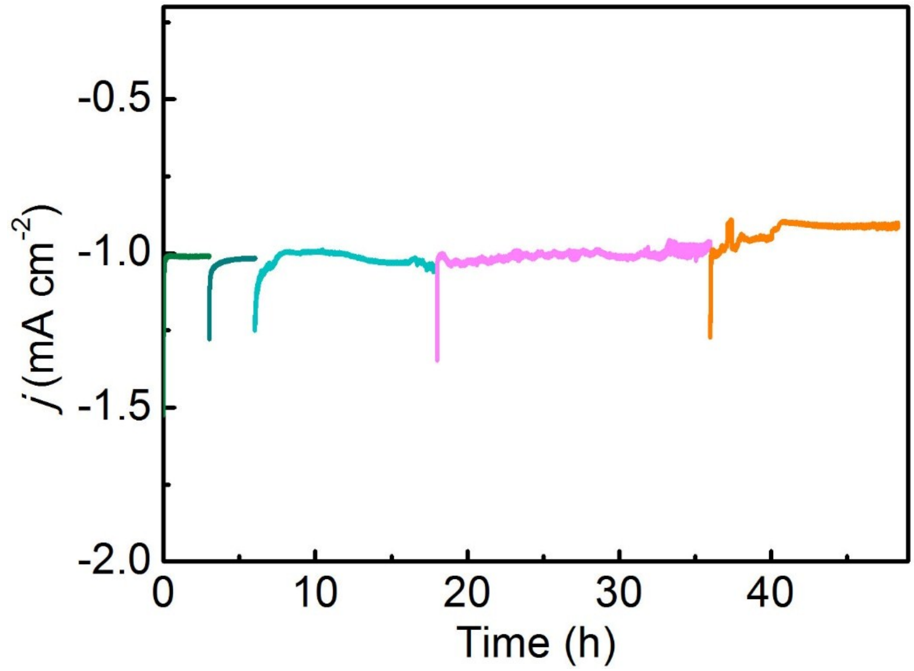

Fig. S11. Chronoamperometric data for d-TiO_2/TM with different time electrolysis using d-TiO_2/TM catalyst in N_2-saturated electrolytes for a total of 48h at –0.15 V.

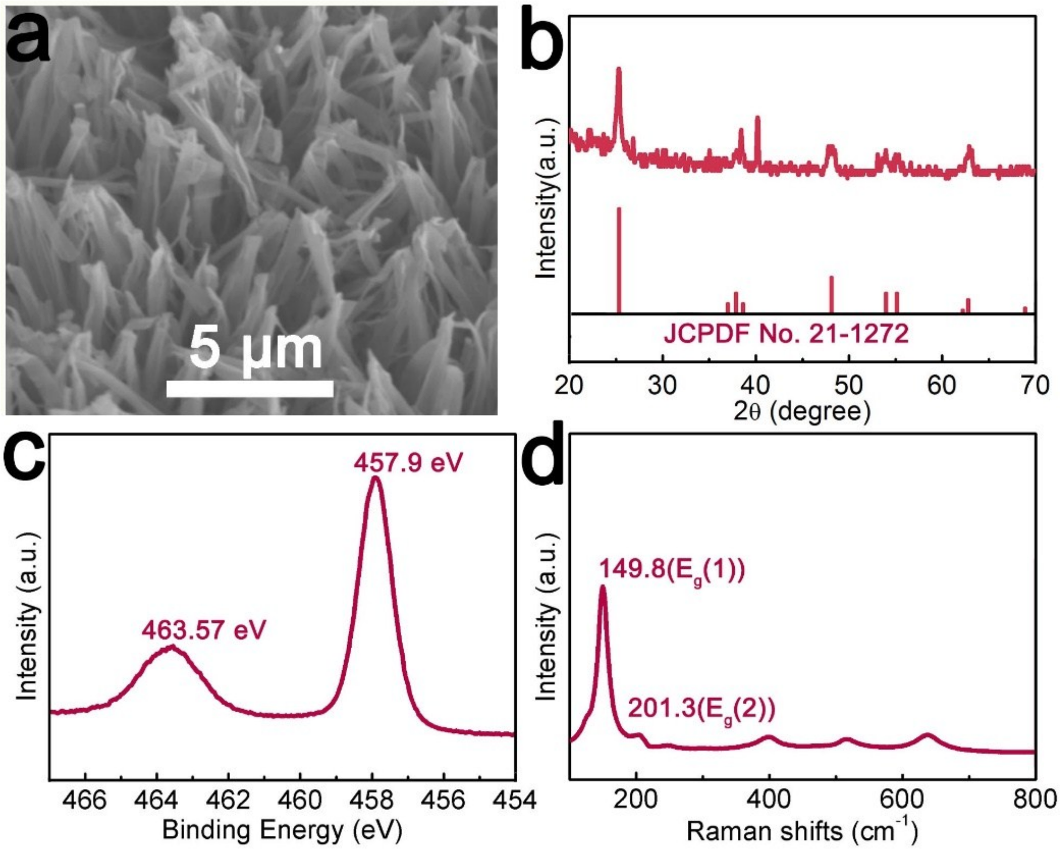

Fig. S12. (a) SEM image of the d-TiO$_2$/TM, (b) XRD pattern of the d-TiO$_2$/TM, (c) XPS spectrum in the Ti 2p region of the d-TiO$_2$ and (b) Raman spectrum of the d-TiO$_2$ after 48h stability test.

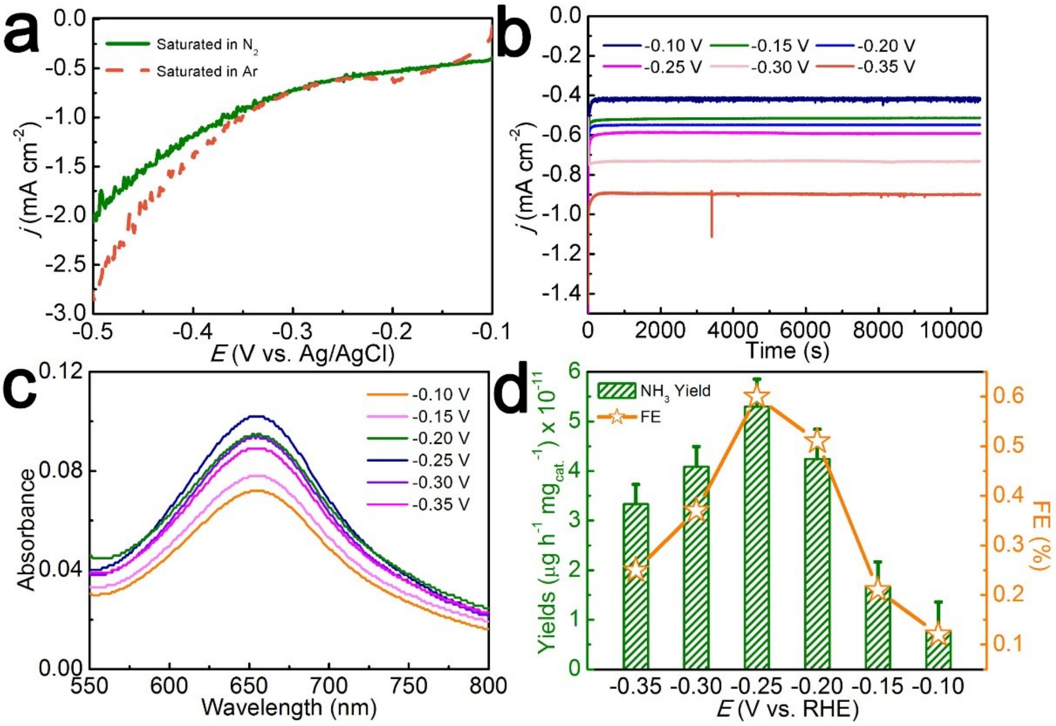

Fig. S13. (a) LSV curves of p-TiO_2/TM in Ar- and N_2-saturated 0.1 M HCl, respectively. (b) Chronoamperometric data of p-TiO_2/TM for NRR at each given potential. (c) UV-Vis absorption spectra of the electrolytes stained with p-$C_9H_{11}NO$ indicator after NRR electrolysis at a series of potentials. (d) NH_3 yields and FEs at each given potential in N_2-saturated 0.1 M HCl. Error bar associated with each value is also provided.

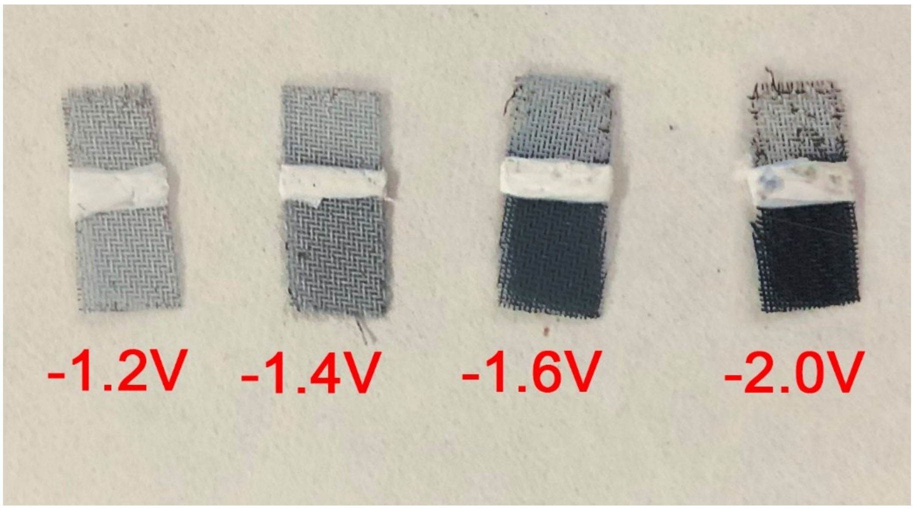

Fig. S14. Optical photograph for different d-TiO_2/TM derived from cathodic polarization under different potentials (from left to right: –1.2 V, –1.4 V, –1.6 V, and –2.0 V (vs. Ag/AgCl)).

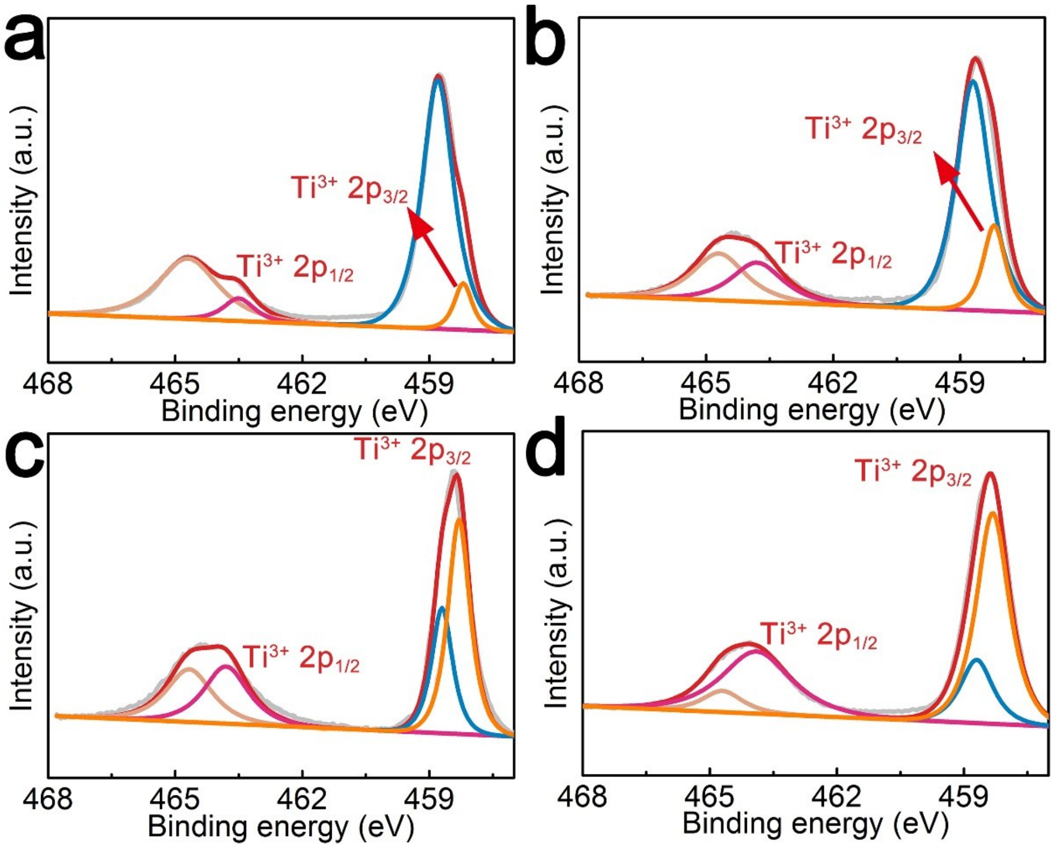

Fig. S15. Ti 2p core-level XPS spectra for different d-TiO_2 derived from cathodic polarization under different potentials: (a) –1.2 V, (b) –1.4 V, (c) –1.6 V, and (d) –2.0 V (vs. Ag/AgCl).

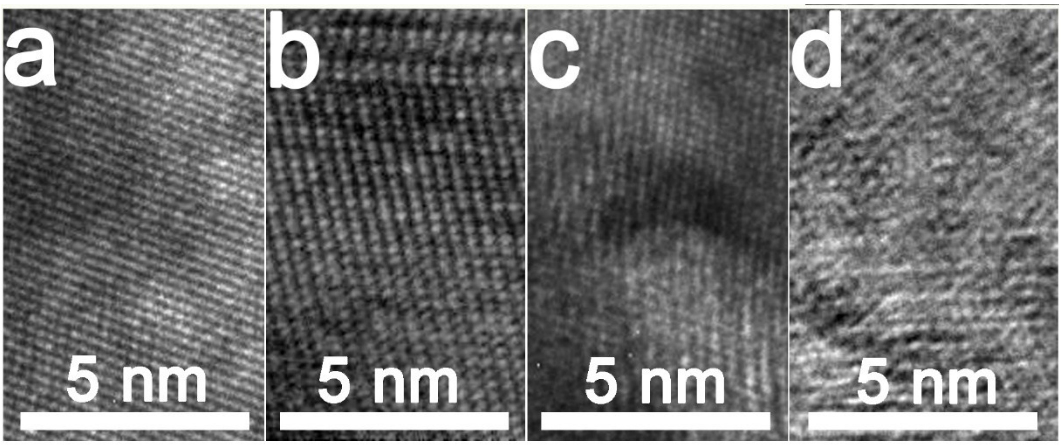

Fig. S16. HRTEM images of for different d-TiO_2 derived from cathodic polarization under different potentials: (a) –1.2 V, (b) –1.4 V, (c) –1.6 V, and (d) –2.0 V (vs. Ag/AgCl).

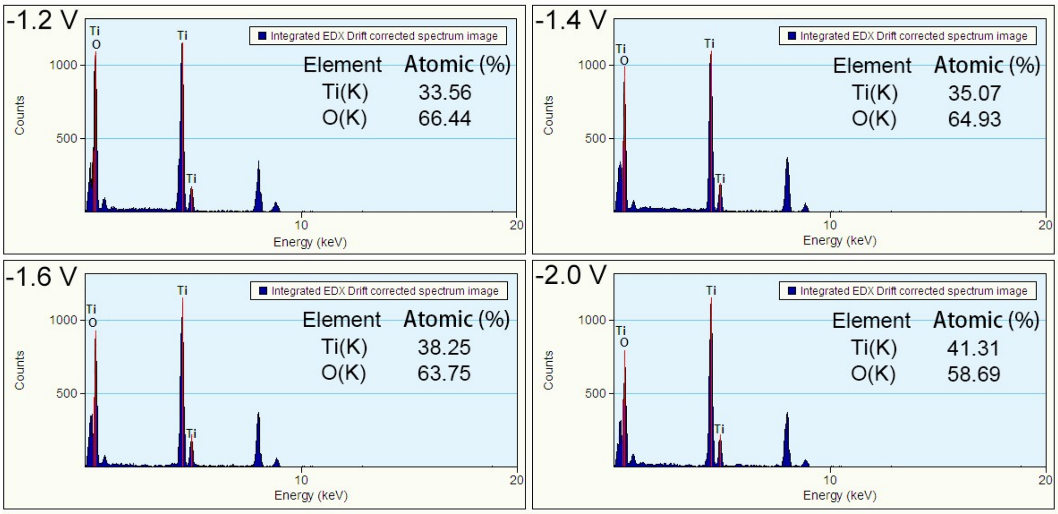

Element	Atomic (%)
Ti(K)	33.56
O(K)	66.44

Element	Atomic (%)
Ti(K)	35.07
O(K)	64.93

Element	Atomic (%)
Ti(K)	38.25
O(K)	63.75

Element	Atomic (%)
Ti(K)	41.31
O(K)	58.69

Fig. S17. Integrated EDX drift corrected spectra of different d-TiO_2 derived from cathodic polarization under different potentials: (a) –1.2 V, (b) –1.4 V, (c) –1.6 V, and (d) –2.0 V (vs. Ag/AgCl).

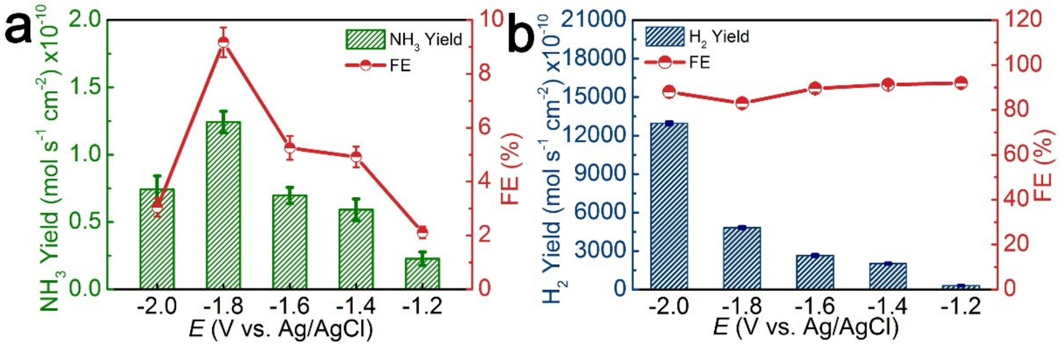

Fig. S18. (a) NH_3 yields and FEs of different d-TiO_2/TM derived from cathodic polarization under different potentials. (b) H_2 yields and FEs of different d-TiO_2/TM derived from cathodic polarization under different potentials. All experiments were carried out at –0.15 V in N_2-saturated 0.1 M HCl at ambient conditions. Error bar associated with each value is also provided.

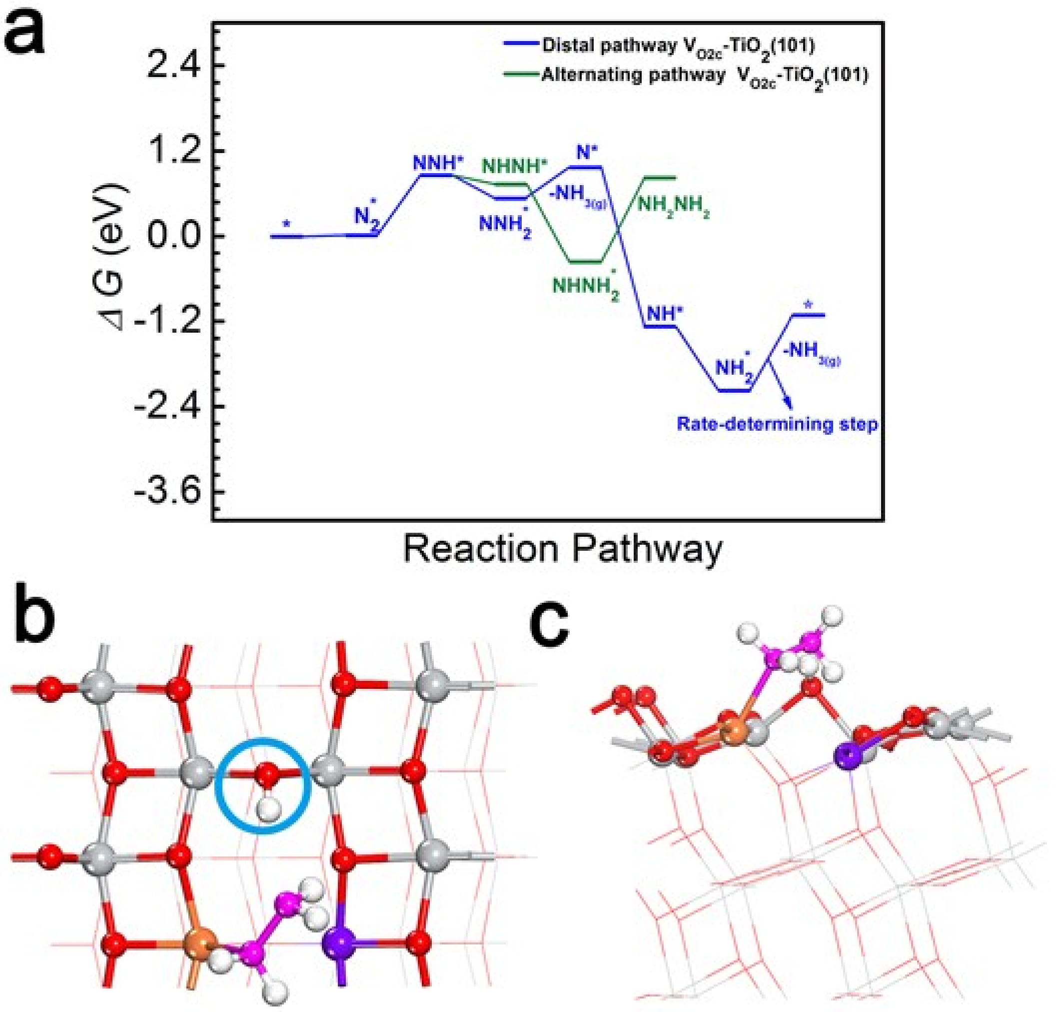

Fig. S19. (a) Free energy diagram with distal and alternating pathways for NRR process on V_{O2c}-TiO_2 (101). For alternating pathway, the rate-determining step is the second NH_3 desorption (reductive adsorption NH_2^* to form $NH_{3(g)}$). (b) and (c) represent top and side view structure of hydrogenation of intermediated $NH_2NH_2^*$ in the alternating pathway on V_{O2c}-TiO_2(101), respectively. Fig. S19a shows that both distal and alternating pathways, the free energy of N_2 ($\Delta G(N_2^*)$) on V_{O2c}-TiO_2(101) surface is only 0.015 eV, but the hydrogenation of the first N atom needs a large $\Delta G(NNH^*)$ of 0.84 eV. In the subsequent steps, it was found that although the value of $\Delta G(NHNH^*)$ in the alternating pathway (green line in Fig. S19a) is slightly higher than that of $\Delta G(NNH_2^*)$ in the distal pathway (blue line in Fig. S19a), it is followed by a quick energy drop with the formation of $NHNH_2^*$. But the hydrogenation of $NHNH_2^*$ ($\Delta G(NH_2NH_2^*)$) is slightly rise by a positive ΔG of

0.15 eV (Fig. S19a), and then hydrogenation of $NH_2NH_2^*$ adsorbs preferentially on the O_{2c} adjacent to V_{O2c} rather than upon $NH_2NH_2^*$(Fig. S19b,c). We also found that the free energy of desorption of $NH_2NH_2^*$ is a positive value of 1.04 eV in Fig. S19a. Overall, these results suggested that the alternating pathway is unexpected on V_{O2c}-TiO_2(101) surface and NH_2NH_2 molecule formation is also difficult. For the distal pathway, the releasing of NH_3 molecular from the hydrogenated NNH_2^* is slightly uphill in the free energy profile by 0.43 eV (blue line in Fig. S19a). But in the subsequent steps, the remaining N^* on the surface will be hydrogenated to NH_2^* by reacting with another two protons coupled with electrons, with a quick free energy drop of –4.12 eV. Finally, the second NH_3 molecule can be desorbed from the V_{O2c}-TiO_2(101) surface after overcoming a positive ΔG of 1.06 eV, in Fig. S19a.

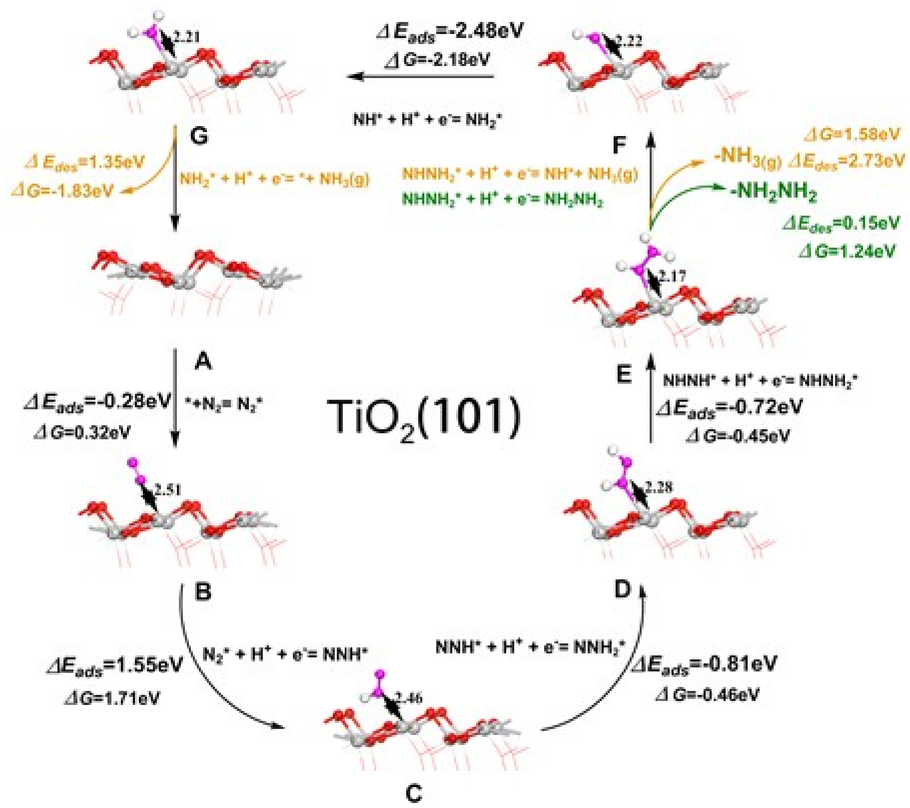

Fig. S20. The mixed pathway atom configurations for NRR on $TiO_2(101)$. Fig. S20 shows the atomic configurations at states of each elementary step on $TiO_2(101)$ surface. The N_2 is in between the surface five and six coordinated Ti atom (denoted as Ti_{4C} and Ti_{5C}, respectively) but tilted to the Ti_{5C} site with a N-Ti_{5C} bond length of 2.51 Å. The hydrogenation of N atom in N_2 follows the alternating mechanism to form $NHNH_2^*$ with a barrier of 2.03 eV. Then, the hydrogenation of $NHNH_2^*$ follows the distal pathway to lead the release of the first NH_3 gas with a positive ΔG of 1.58 eV. In the subsequent steps, the remaining NH* on the surface will be hydrogenated to the second NH_3 gas by reacting with another two protons coupled with electrons, with a quick free energy drop of –4.01 eV.

Table S1. Comparison of the electrocatalytic NRR performance of d-TiO_2/TM with other aqueous-based NRR electrocatalysts at ambient conditions.

Catalyst	**Electrolyte**	**NH_3 yield rate (mol s^{-1} cm^{-2})**	**FE(%)**	**Ref.**
d-TiO_2/TM	**0.1 M HCl**	**1.24×10^{-10}**	**9.17**	**This work**
Au nanorods	0.1 M KOH	2.69×10^{-11}	3.88	1
$Bi_4V_2O_{11}$/CeO_2	0.1 M HCl	3.79×10^{-10}	10.16	2
(110)-oriented Mo nanofilm	0.01 M H_2SO_4	3.09×10^{-11}	0.72	3
Ru/Ti	0.5 M H_2SO_4	1.19×10^{-10}	--	4
MoS_2/CC	0.1 M HCl	8.48×10^{-11}	0.096	5
	0.1 M $NaSO_4$	8.08×10^{-11}	1.17	
PEBCD/C	0.5 M Li_2SO_4	2.58×10^{-11}	2.85	6
AuHNCs	0.5 M $LiClO_4$	6.37×10^{-11}	30.2	7
N-doped carbon nanospikes	0.25 M $LiClO_4$	1.59×10^{-9}	11.56	8
Fe_2O_3-CNT	diluted $KHCO_3$	3.58×10^{-12}	0.15	9
C-ZIF-1100-1h	0.1 M KOH	9.44×10^{-10}	10.2	10
MoO_3	0.1 M HCl	4.80×10^{-10}	1.9	11
Fe_3O_4/Ti	0.1 M Na_2SO_4	5.6×10^{-11}	2.6	12
MoN	0.1 M HCl	3.01×10^{-10}	1.15	13
VN	0.1 M HCl	8.40×10^{-11}	2.25	14
TiO_2	0.1 M Na_2SO_4	9.16×10^{-11}	2.5	15
TiO_2-rGO	0.1 M Na_2SO_4	9.89×10^{-11}	3.3	16
C-doped TiO_2 nanoparticles	0.1 M Na_2SO_4	2.65×10^{-11}	1.84	17
Boron-Doped TiO_2	0.1 M Na_2SO_4	2.35×10^{-11}	3.4	18

Reference

1. D. Bao, Q. Zhang, F. Meng, H. Zhong, M. Shi, Y. Zhang, J. Yan, Q. Jiang and X. Zhang, *Adv. Mater.*, 2017, **29**, 1604799.
2. C. Lv, C. Yan, G. Chen, Y. Ding, J. Sun, Y. Zhou and G. Yu, *Angew. Chem., Int. Ed.*, 2018, **57**, 6073–6076.
3. D. Yang, T. Chen and Z. Wang, *J. Mater. Chem. A*, 2017, **5**, 18967–18971.
4. K. Kugler, M. Luhn, J. A. Schramm, K. Rahimi and M. Wessling, *Phys. Chem. Chem. Phys.*, 2015, **17**, 3768–3782.
5. L. Zhang, X. Ji, X. Ren, Y. Ma, X. Shi, Z. Tian, A. M. Asiri, L. Cheng, B. Tang and X. Sun, *Adv. Mater.*, 2018, **30**, 1800191.
6. G. Chen, X. Cao, S. Wu, X. Zeng, L. Ding, M. Zhu and H. Wang, *J. Am. Chem. Soc.*, 2017, **139**, 9771–9774.
7. M. Nazemi, S. R. Panikkanvalappil and M. A. El-Sayed, *Nano Energy*, 2018, **49**, 316–323.
8. Y. Song, D. Johnson, R. Peng, D. K. Hensley, P. V. Bonnesen, L. Liang, J. Huang, F. Yang, F. Zhang, R. Qiao, A. P. Baddorf, T. J. Tschaplinski, N. L. Engle, M. C. Hatzell, Z. Wu, D. A. Cullen, H. M. Meyer III, B. G. Sumpter and A. J. Rondinone, *Sci. Adv.*, 2018, **4**, e1700336.
9. S. Chen, S. Perathoner, C. Ampelli, C. Mebrahtu, D. Su and G. Centi, *Angew. Chem., Int. Ed.*, 2017, **56**, 2699–2703.
10. S. Mukherjee, D. A. Cullen, S. Karakalos, K. Liu, H. Zhang, S. Zhao, H. Xu, K. L. More, G. Wang and G. Wu, *Nano Energy*, 2018, **48**, 217–226.

11. J. Han, X. Ji, X. Ren, G. Cui, L. Li, F. Xie, H. Wang, B. Li and X. Sun, *J. Mater. Chem. A*, 2018, **6**, 12974–12977.
12. Q. Liu, X. Zhang, B. Zhang, Y. Luo, G. Cui, F. Xie and X. Sun, *Nanoscale*, 2018, **10**, 14386–14389.
13. L. Zhang, X. Ji, X. Ren, Y. Luo, X. Shi, A. M. Asiri, B. Zheng and X. Sun, *ACS Sustainable Chem. Eng.*, 2018, **6**, 9550–9554.
14. R. Zhang, Y. Zhang, X. Ren, G. Cui, A. M. Asiri, B. Zheng and X. Sun, *ACS Sustainable Chem. Eng.*, 2018, **6**, 9545–9549.
15. R. Zhang, X. Ren, X. Shi, F. Xie, B. Zheng, X. Guo and X. Sun, *ACS Appl. Mater. Interfaces*, 2018, **10**, 28251–28255.
16. X. Zhang, Q. Liu, X. Shi, A. M. Asiri, Y. Luo, T. Li, X. Sun, *J. Mater. Chem. A*, 2018, **6**, 17303–17306.
17. K. Jia, Y. Wang, Q. Pan, B. Zhong, Y. Luo, G. Cui, X. Guo and X. Sun, *Nanoscale Adv.*, 2018, DOI: 10.1039/C8NA00300A.
18. Y. Wang, K. Jia, Q. Pan, Y. Xu, Q. Liu, G. Cui, X. Guo and X. Sun, *ACS Sustainable Chem. Eng.*, 2018, DOI: 10.1021/acssuschemeng.8b05332.